Fuel 331 (2023) 125851

Contents lists available at ScienceDirect

Fuel

journal homepage: www.elsevier.com/locate/fuel

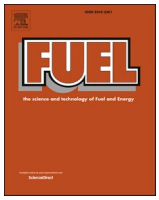

Full Length Article

Particle collection and heavy metals migration during high-temperature electrostatic precipitation in copper smelting: A pilot-scale study

Zhicheng Wu [a], Dingzhen Wang [a], Yifan Wang [a], Lingyu Shao [a], Yuzhong He [b], Hui Liu [c], Chenghang Zheng [a,*], Xiang Gao [a]

[a] State Key Lab of Clean Energy Utilization, State Environmental Protection Engineering Center for Coal-Fired Air Pollution Control, Zhejiang University, 38 Zheda Road, Hangzhou 310027, People's Republic of China
[b] Zhejiang Feida Environmental Science & Technology Co., Ltd., Zhuji 311800, Zhejiang Province, People's Republic of China
[c] Chinese National Engineering Research Center for Control & Treatment of Heavy Metal Pollution, Central South University, Changsha 410083, People's Republic of China

ARTICLE INFO

Keywords:
Heavy metals collection and migration
PM removal characteristics
High-temperature electrostatic precipitation in copper smelting
Pilot scale

ABSTRACT

Recently, large amounts of particulate matter (PM) and heavy metals (HMs) have been generated in the processes of non-ferrous metal smelting (NFMS). High-temperature electrostatic precipitator (HT-ESP) was the key method to capturing PM while extensive HMs enriched. In this work, the PM collection and migration of HMs in the HT-ESP process of copper smelting were investigated through an established pilot-scale platform. The excellent performance of the pilot-scale HT-ESP could achieve a particle collection efficiency of 99.5 %. The distribution patterns of HMs in various particle sizes revealed that the volatile heavy metals, arsenic (As) and selenium (Se) were predominantly distributed in $PM_{1.0}$ and $PM_{1\text{-}2.5}$ with a moderately dispersed distribution, whereas copper (Cu) and lead (Pb) were densely concentrated on particles. When the temperature difference between the inlet and the outlet of the HT-ESP narrowed to 23 K, the original As and Se enriched in hopper particles partially volatilized and migrated into the gas phase and adhered to tiny size particles. The enrichment ratio in the gas phase (ER_G) of As and Se increased by 2.7 % and 18.5 %, respectively. The results were beneficial to reducing the enrichment of volatile HMs in copper smelting ash and provided guidance for resource utilization of the copper smelting industry.

1. Introduction

The nonferrous metal smelting (NFMS) process is considered one of the main sources of large amounts of particulate matter (PM) and many hazardous heavy metals (HMs, including As, Se, Cd, Cr, Pb, Hg, etc.) [1–4]. In the process of calcination and smelting of copper-nickel sulfide mine, these HMs tend to enter the flue gas after vaporization or sublimation at high temperatures [5,6]. As the flue gas temperature decreases, arsenic and some other volatile heavy metals condense into the PM [7]. These PM enriched with toxic heavy metals will cause serious adverse effects on human health and the environment if they can not be treated effectively (Anjum et al., 2021; Kumar et al., 2020). Therefore, achieving the effective removal of PM and the separation of PM and HMs at high temperatures is imperative [8,9].

Electrostatic precipitator (ESP) is a significant high-temperature PM removal technology and has been widely applied for collecting fine PM in many industries including NFMS with its advantages of low-pressure drop and energy consumption [10,11]. Flue gas atmosphere, operating voltage, flow rate, and particle properties are considered the key factors affecting the collection efficiency of ESPs operating at high temperatures [12,13]. Many researchers have found that high temperature limited the range of operating voltage, and the decrease of applied voltage at high temperature led to the reduction of particle charging electric field force, resulting in small particles being difficult to capture [14,15]. A few researchers investigated the effect of flue gas atmosphere on corona discharge at high temperatures and claimed that high concentrations of electronegative gases (such as SO_2, CO_2, etc.) can inhibit the discharge current [16]. If the proportion of electronegative gas was higher, the ion generation rate and mobility would be lower, and the particle charge would be lower, leading to a lower PM collection efficiency [17,18]. Meanwhile, the process of PM removal in ESP involves the collection, enrichment, and migration of heavy metals. According to previous

* Corresponding author.
E-mail address: zhengch2003@zju.edu.cn (C. Zheng).

https://doi.org/10.1016/j.fuel.2022.125851
Received 25 June 2022; Received in revised form 12 August 2022; Accepted 26 August 2022
Available online 13 September 2022

investigations related to coal combustion, the emission concentration of HMs at coal-fired power plants was usually below 5 μg/m^3 [19,20]. Previous studies also revealed that HMs were more likely to be concentrated in particles with small particle sizes [21–23]. The finer PM captured by ESP had the highest concentration of HMs with increased mobility of Se, Cd, and Pb among ultralow emission air pollution control devices [24].

However, the atmosphere of the nonferrous metal smelting flue gas was complex with extremely high sulfur oxides (0.1–0.3 t/d [25]), and PM emitted from NFMS processes contain high concentrations of arsenic, which was quite different from that emitted from coal combustion [26]. Only a few studies have been conducted on the emission of HMs during nonferrous metal smelting, while fewer studies focused on the copper smelting process compared to Zn/Pb smelting [27,28]. Recently, the emission characteristics of PM and heavy metals in flue gas generated from a typical copper smelting plant and the emission factors were revealed by limited research [29]. Whereas the migration and collection of HMs in the gas and solid phases during the high-temperature electrostatic precipitator process of copper smelting still lacks in-depth research. Therefore, how to improve the collection efficiency of PM in the high-temperature ESP process of NFMS and reveal the collection and migration of the HMs is the focus of current research.

In this study, a self-designed high-temperature ESP (HT-ESP) pilot-scale platform was built in a typical copper smelting plant in China. Based on such a platform, the PM removal characteristics of high-temperature ESP under different applied voltage and flow rate operating conditions were studied. Moreover, the migration and enrichment proportion of HMs in the gas phase and PM during high-temperature electrostatic precipitation were further analyzed. The results achieved a particle collection efficiency exceeding 99.5 % under the optimal flue gas flow rate and maximum voltage. Furthermore, a method of reducing the enrichment of toxic HMs in hopper particles was proposed, which was beneficial to improving the removal of HMs in the subsequent acid production system and has a guiding significance for realizing resource utilization.

2. Methodology

2.1. HT-ESP pilot-scale platform and smelting process description

To obtain the collection and migration characteristics of PM and HMs during high-temperature electrostatic precipitation under the actual copper smelting flue gas with high PM and SO_2 concentration, a typical copper smelting plant in China was chosen as the site for this study. The type of copper smelting process in this plant was suspension smelting with a flash furnace. The flash furnace smelting process has the advantages of a large production capacity and low energy consumption [30]. The annual output of the copper cathode for the abovementioned copper smelting plant exceeded 300,000 tons/yr.

The specific copper smelting and pollutants treatment process is illustrated in Fig. 1a. The copper concentrate, slag, and circulated flue dust were mixed in a certain proportion and sent to the dry ore bin through the conveyor belt. Then the mixture in the dry ore bin was fed into the flash furnace by the concentrated nozzle. After smelting, it could produce slag, about 70 % copper matte, and a large amount of dust-containing off-gas with high temperature and high SO_2 concentration. The dust-containing off-gas produced by the flash furnace entered the waste heat boiler (WHB) for cooling and coarse ash removal. Subsequently, the flue gas entered the HT-ESP through a dust settling chamber (DSC) for fine PM removal and the rest of the flue gas was mixed into the acid production system. Meanwhile, the captured fly ash in such a process was transported by the ash delivery system to the flash smelting

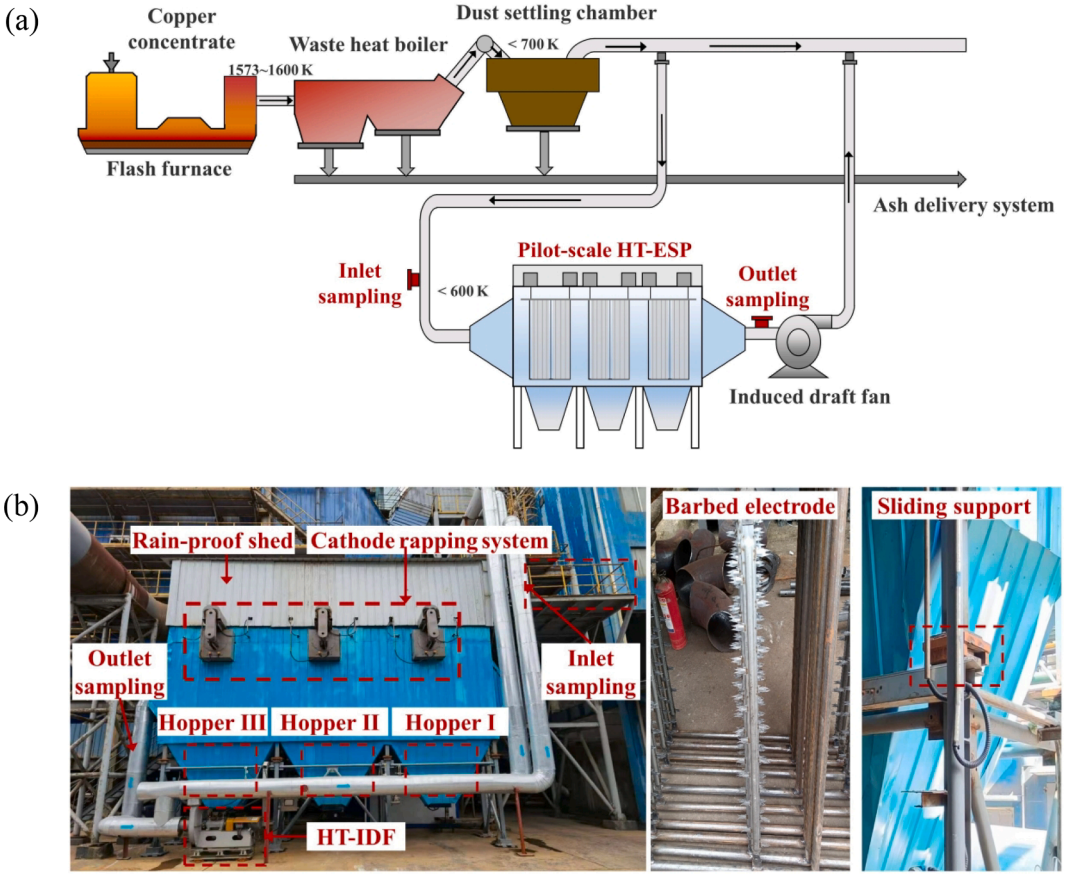

Fig. 1. The copper smelting process and the pilot-scale HT-ESP platform (a) schematic (b) field photographs.

furnace and blowing furnace top soot bins respectively.

Compared with the original ESP in the copper smelting plant, the HT-ESP platform in this study has the following advantages:

1. the flue gas velocity could be altered by adjusting the frequency of the induced draft fan;
2. a reinforced flexible graphite barbed discharge electrode was adopted, and the current density was significantly larger than the original wire electrode at the temperature within 600 K based on our previous experimental study.[31];
3. a sliding support structure was adopted to solve the dimensional expansion caused by the long-term high-temperature operation of the original ESP, thereby reducing the air leakage rate and improving the PM collection efficiency;
4. the closer distance between the inlet and outlet sampling positions made sampling more convenient, which was conducive to revealing the migration and collection mechanism of PM and HMs.

The field photographs of the platform are displayed in Fig. 1b. The pilot-scale HT-ESP was mainly composed of high-frequency power supplies, metal anode plates, barbed discharge electrode, a rapping system, a rain-proof shelter, and a high temperature-induced draft fan (HT-IDF). It had the structure of a chamber a three-stage electric field, the first-stage electric field had four channels, and the latter two-stage electric field had three channels. The rated flue gas flow of the platform was set to 2600 m^3/h and specific key parameters are listed and compared in Table 1. These parameters were also compared with the original ESP and another industrial HT-ESP [32] listed in Table S1. And the PM collection efficiency of the pilot-scale HT-ESP could be effectively enhanced. In this study, the flue gas velocity could be altered by changing the frequency of HT-IDF, and the calibration of HT-ITF is shown in Fig. S1a. In addition, the applied voltage of each electric field could be changed by adjusting the high-frequency power supply. The discharge characteristics of different power supplies with different stages of the electric field at room temperature are shown in Fig. S1b.

2.2. Sampling methods

The flue gas sampling sites were located at the inlets and outlets of the pilot-scale HT-ESP (Fig. 1). The sampling system was designed based on the method of condensation combined with absorption according to EPA Method 29 [33] (Fig. 2).

2.2.1. PM sampling

To obtain representative PM samples from the flue gas, isokinetic sampling was a very important process. In this work, an isokinetic sampling probe with heating functions was utilized to ensure that the sampling velocity was consistent with the flue gas velocity at the sampling point, and the relative error was kept within 5 %. In addition, to avoid HMs condensing on the isokinetic sampling probe, it had to be pre-heated close to the flue gas temperature at the sampling point. Due to the high temperature (>550 K) and high PM concentration at the inlet, quartz fiber filter cartridges were installed at the front of the isokinetic sampling probe to capture the inlet PM and filter the solid phase in the flue gas. For outlet PM sampling, in addition to using quartz fiber filter cartridges, a four-stage inertial impactor (Dekati® PM10 Impactor, Finland) was applied to investigate the enrichment and removal characteristics of HMs on PM with different particle sizes. The PM10 impactor classified PM into four size fractions under the action of gravity and inertial. Four collection stages were arranged in sequence from top to bottom to capture particle size >10 μm ($PM_{>10}$), 2.5–10 μm ($PM_{2.5-10}$), 1–2.5 μm ($PM_{1-2.5}$), and particle size <1 μm ($PM_{1.0}$) particles. Collection substrates were placed on the collection plates. These substrates were weighed before and after the measurement to obtain information on particle mass size distribution. The aluminum foil membranes with a low blank value of HMs were selected as collection substrates and should be greased with Apiezon-L before the measurement to prevent particle bounce (Fig. S2).

Table 1
Key parameters of the pilot-scale HT-ESP platform.

Devices	Items	Unit	Value
HT-ESP	Treated flue gas flow	m^3/h	1000–4800
	Treated temperature	K	550–600
	Field stage	–	3
	Chamber	–	1
	Effective length of the field	m	3 × 2
	Effective height of the field	m	1.50
	Air leakage rate	%	<2
	Design resistance	Pa	<250
	Specific collection area	$m^2/(m^3/s)$	99.7–265.8
	Gas velocity	m/s	0.24–0.64
	Distance between collection plate	mm	1st stage: 400 2nd/3rd stage: 300

2.2.2. Gas phase sampling

The gas phase after filtration was condensed by the condensing unit and then extracted by the absorbent in a series of impingers. The condensing unit was composed of a reflux condenser and a micro-submersible pump. The micro submersible pump accelerated the condensation of high-temperature flue gas by circulating the ice-water mixture. The absorbent in the first and second impinger was excess 20 wt% NaOH solution, they were used to absorb the excessive amount of SO_2 (>20 wt%)) and arsenic-containing oxides in the gas phase. While the third and the fourth impinger, containing 5 wt% HNO_3/10 wt% H_2O_2 solution, were conducted to measure the concentration of HMs including As, Pb, Cd, Cr, and Se in the gas phase. Additionally, the last impinger was equipped with silica gel to absorb the vapor in the flue gas and prevent moisture from entering the vacuum pump. Teflon tapes were used for sealing adjacent impingers to insure leak-free sampling train connections.

2.3. Quality assurance and analytical method

The sampling devices needed to be pretreatment before sampling. The quartz fiber cartridges were pre-heated at 550–600 K for 3 h before blank weighing to eliminate the weight loss under the high-temperature flue gas. Also, the sampling probe and PM10 impactor were preheated at the same temperature for over 15 min to ensure the stability of sampling. To minimize the underestimation of the HMs content in the gas phase caused by vapor condensation onto pipes, the connecting pipes were replaced with new ones after each sampling, and the removed pipes were cleaned with absorbents and the HMs content was also detected. In addition, HMs in both solid and gas phases were sampled three times at the inlets and the outlets of HT-ESP to verify data quality and limit the possible fluctuation owing to the variation of raw material smelting. [29].

2.3.1. PM measurements

The morphology of the sampling PM was tested by scanning electron microscope (SEM, SU70, and SU-8010) with energy dispersive spectroscopy (EDS), and the content of elements was tested by X-ray fluorescence (XRF) while the particle size distribution was tested by a laser particle size analyzer (Mastersizer 3000). The inlet or outlet PM mass concentration could be obtained by calculating the weight difference of the quartz fiber filter cartridge or aluminum films before and after sampling, and then dividing by the amount of flue gas. The sampling flow and sampling time of the PM and gas phase were fixed and the same for each working condition, and the PM mass concentration of each working condition was measured three times to reduce errors. The calculating formula is as follows:

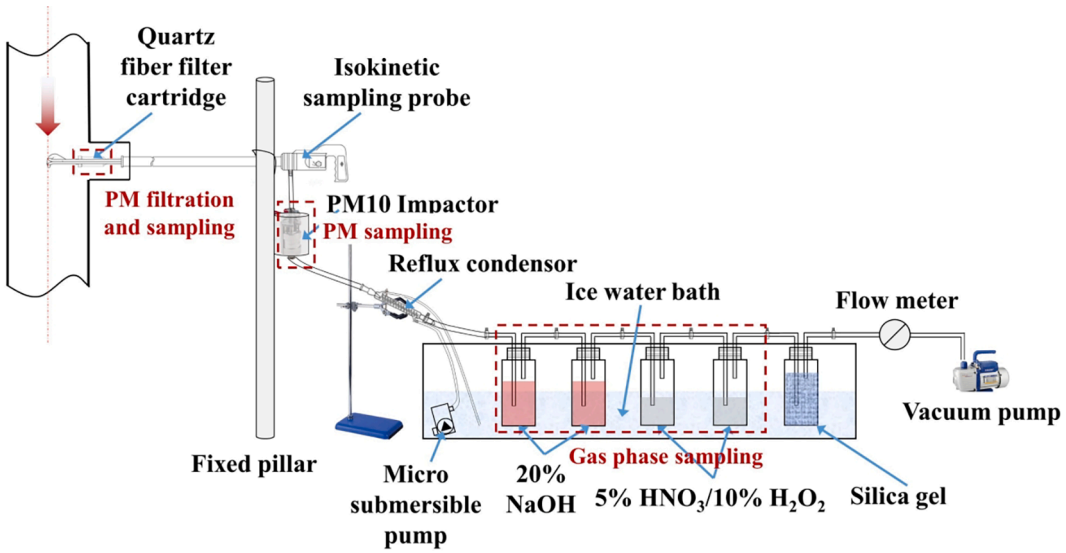

Fig. 2. The sampling system of copper smelting flue gas.

$$C_{S,inlet} = \frac{m_{inlet} - m_{0,inlet}}{Q} \quad (1)$$

$$C_{S,outlet} = \frac{m_{outlet} - m_{0,outlet}}{Q} \quad (2)$$

$$\eta = \frac{C_{S,inlet} - C_{S,outlet}}{C_{S,inlet}} \times 100\% \quad (3)$$

where $C_{S,inlet}$ and $C_{S,outlet}$ represent the inlet and outlet particle mass concentration, mg/m^3; m_{inlet}, m_{outlet} is the weight of quartz fiber cartridges and membranes after sampling while m_0 is the blank weight, mg, η is the PM collection efficiency of the HT-ESP, %; Q is the sampling flue gas flow, m^3.

2.3.2. HMs concentration measurements

According to the gas phase sampling, HMs entering the gas phase were absorbed by the solution in the impingers. The content of these HMs emissions was analyzed by inductively coupled plasma-mass spectroscopy (ICP-MS, PerkinElmer NexION 300X, Agilent Technologies 7800) directly after filtration and dilution. However, the process of obtaining the emission of HMs in PM with different particle sizes was relatively complicated. The sampled quartz fiber cartridges and aluminum foil membranes were digested in a Teflon digester. The specific digestion steps were to weigh the same mass of samples into a Teflon digestion tank, added 2 ml of HF and 8 ml of HNO_3 and then heated for 2 h. After the digestion was complete, a vapor block was used to drive the acid for one hour, and then the digestion liquid was poured into a 50 ml volumetric flask and made up to volume with deionized water. The HMs content in the solution was then measured by ICP-MS and the content of HMs in PM could be obtained by conversion.

Compared with particles in the ash hopper, the mass of the particles on the discharge electrode and collecting plate could be ignored approximately, therefore the hopper ash mass concentration could be obtained by the difference value between the inlet and outlet mass concentration under the same sampled flue gas volume. According to the mass balance in which the input of HMs is equal to the output HMs in the HT-ESP, the calculating formulas of HMs concentration in particles and gas phase at different locations of HT-ESP are as follows:

$$C_{Si,inlet} = C_{S,inlet} \times X_{i,inlet} \quad (4)$$

$$C_{Si,outlet} = C_{S,outlet} \times X_{i,outlet} \quad (5)$$

$$C_{Gi,inlet} = \frac{N_{i,inlet} \times D_{ri,inlet} \times V}{Q} \quad (6)$$

$$C_{Gi,outlet} = \frac{N_{i,outlet} \times D_{ri,outlet} \times V}{Q} \quad (7)$$

$$m_{Si,hopper} = m_{Si,inlet} + m_{Gi,inlet} - m_{Si,outlet} - m_{Gi,outlet} \quad (8)$$

$$C_{Si,hopper} = C_{Si,inlet} + C_{Gi,inlet} - C_{Si,outlet} - C_{Gi,outlet} \quad (9)$$

where m_{Si} and m_{Gi} represent the distribution of various HMs mass in solid and gas phase, mg; C_{Si} and C_{Gi} represent the distribution of various HMs mass concentration in solid and gas phase, mg/m^3; X_i, N_i represent the mean proportion of a certain TE in particle and gas absorption solvent, μg/g, ug/l; V is the constant volume, l; and D_r is the dilution ratio.

3. Results and discussion

3.1. Removal characteristics of PM during HT-ESP

The flue gas velocity and applied voltage had a great impact on PM removal by conventional ESPs. The inlet and outlet particle mass concentration variation of the HT-ESP process with flue gas velocity is displayed in Fig. 3. When the flue gas velocity was low (<0.5 m/s), the increase of inlet PM concentration was modest, and when the flue gas velocity was high, the inlet PM concentration fluctuated drastically with a large standard deviation (Fig. 3a). The variation trend of PM concentration at the outlet of the HT-ESP with flue gas velocity was roughly the same as that of inlet PM concentration (Fig. 3b). It was found that when the HT-ESP was operating under rated conditions (the three-stage electric field strength was kept around 2.3 kV/cm), there was an optimum flue gas velocity (0.48 m/s) for maximum particle collection efficiency. The maximum PM collection efficiency exceeding 98 % could be obtained at this time. A possible reason was when the flow rate was low, the inlet mass concentration was small, and the mass concentration was positively correlated to the collection efficiency, thus the flow rate and the collection efficiency were not negatively correlated. Furthermore, we found that a low flow rate could lead to rapid and massive deposition of PM in the collecting plate to form a dust layer leading to blockage and more likely to cause breakdown to reduce PM collection efficiency. With the further increase of the flue gas velocity, many particles escaped from the electric field before being captured, resulting in a dramatic drop in collection efficiency. Therefore, ensuring the flue gas velocity in the HT-

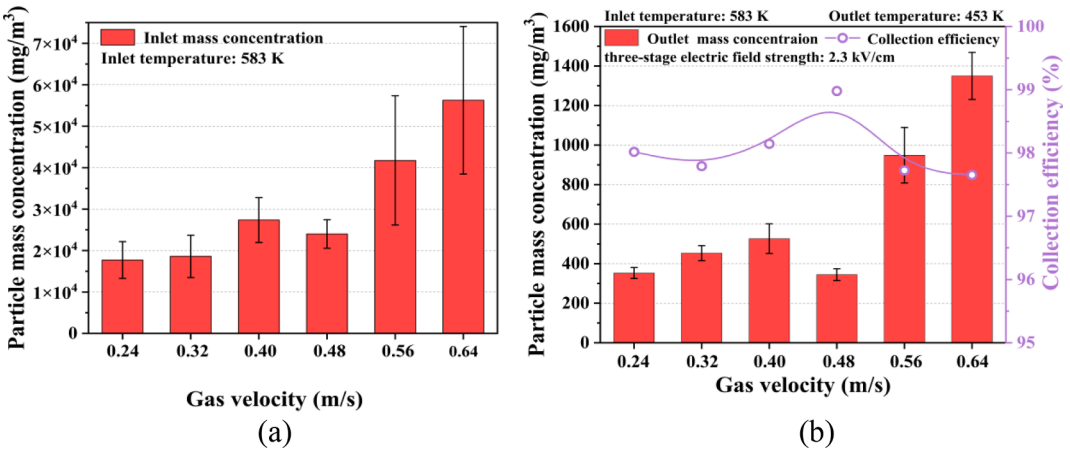

Fig. 3. Particle mass concentration under different flue gas velocities. (a) inlet mass concentration (b) outlet mass concentration and collection efficiency.

ESP in a suitable range was significant to improve the collection efficiency of NFMS particles.

The applied voltage is another important factor affecting the collection effect of ESP. The particle mass concentration at the outlet of HT-ESP under different stages of electric field and the applied voltage is shown in Fig, 4. When the first electric field was operating under rated conditions, with the increase of the second electric field voltage, the particle mass concentration decreased significantly, and the collection efficiency increased (Fig. 4a). By increasing the first electric field voltage to 60 kV and maintaining the second electric field constant at 35 kV, the lowest average outlet mass concentration (114.2 mg/m^3) and the highest collection efficiency (99.5 %) could be obtained (Fig. 4b). In addition, it could be found from Fig. 4c and Fig. 4d that particle size smaller than 2.5 μm occupied a large fraction of the outlet mass concentration. The possible reason could be attributed to fine particles absorbing a large amount of sulfate and condensable PM in the flue gas caused by a large temperature drop. Simultaneously, some local large particles could collide and bounce to the $PM_{1\text{-}2.5}$ and $PM_{1.0}$ membranes.

3.2. *Distribution of HMs in particles at different locations of HT-ESP*

Based on the abovementioned PM removal characteristics, to figure out the distribution of heavy metals in the PM during the HT-ESP process, the main chemical composition of the copper smelting PM at different locations of the HT-ESP under rated operating conditions was tested by XRF, and the results are listed and compared in Table 2. The

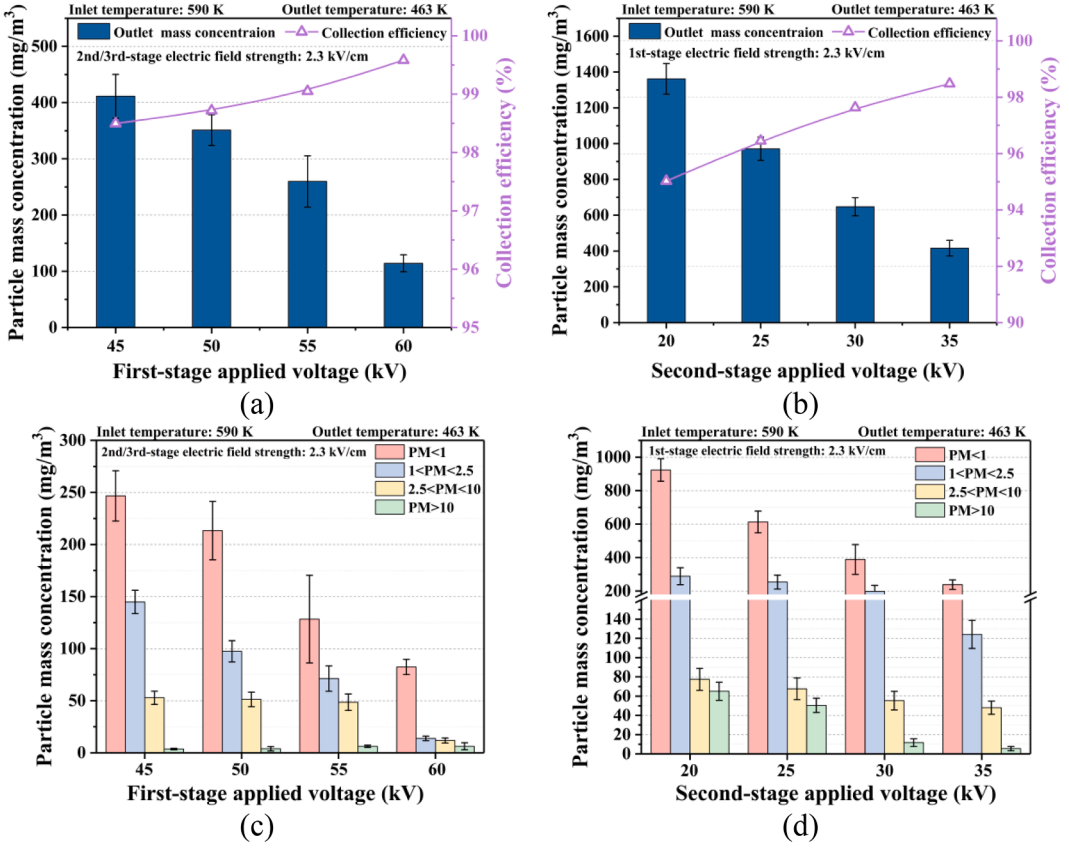

Fig. 4. Total outlet particle mass concentration and collection efficiency under different applied voltage and electric field stages (a) first-stage (b) second-stage; Fractional outlet particle mass concentration under different applied voltage and electric field stages (c) first-stage (d) second-stage.

Table 2
Mean chemical composition of PM at different locations of the HT-ESP under rated operating conditions (wt%).

Element	Inlet	Ash hopper			Outlet				
		I	II	III	Total	$PM_{>10}$	$PM_{2.5-10}$	$PM_{1-2.5}$	$PM_{1.0}$
O	43.39	42.65	42.02	41.34	40.58	44.43	43.15	39.89	40.54
Si	2.98	2.69	2.21	2.97	2.45	2.48	2.65	3.19	3.39
S	9.42	9.81	11.18	10.93	14.37	13.51	14.48	15.22	16.11
Fe	11.82	11.75	10.48	9.51	11.16	12.24	11.58	12.07	10.24
Cu	16.71	15.62	17.09	16.34	16.04	15.27	16.06	14.34	11.67
Zn	5.19	5.44	4.25	3.12	4.06	2.04	1.65	2.76	4.36
As	6.46	7.65	8.68	9.98	7.36	5.91	6.57	8.11	7.60
Pb	2.15	2.32	2.49	3.38	2.04	2.56	1.64	1.46	0.76
Se	ND	0.02	0.04	0.07	0.05	ND	ND	0.13	0.37

distribution of elements was similar to previously conducted research [34,35]. The PM in the outlet and the hopper of HT-ESP was found to have a high weight percentage of copper content, with an average of over 15 %. For other heavy metals, the content of arsenic and lead was relatively high, especially the content of arsenic could reach up to 9.98 %, manifesting high toxicity of the copper smelting ash. Moreover, it seemed that arsenic was more enriched in particles of hopper III than that of hopper I and hopper II. In addition, the content of selenium in inlet particles was below the detection range (indicated as ND in Table 2), indicating that there was almost no selenium enrichment in inlet particles. However, the content of selenium was detected in the outlet and hopper particles. The reason could be attributed to the existence of temperature difference between the inlet and the outlet of the HT-ESP, and the lowering of temperature promotes the enrichment of volatile selenium in the particles.

To confirm the specific distribution of HMs in particles of ash hoppers, the size distribution and morphology of particles in different hoppers were firstly analyzed by SEM and EDS in Fig. 5a. The copper smelting PM in the HT-ESP hopper had a bimodal distribution and the morphology was aspherical with stacked flake and block structures, which was quite different from the particle size distribution of other industries [36]. Since the dust-laden flue gas first entered the first-stage electric field, most of the large particles were captured into the hopper I, resulting in a large median particle size of 145 μm (Dv(50) = 145 μm) for particles in the hopper I. The size distribution of particles in the hopper II was similar to that in the hopper III, the median particle size was 28.3 μm and 26.9 μm, respectively. According to the EDS mapping of HMs in hopper ash (Fig. 5b), the distribution of copper and lead was dense on the particles, indicating copper and lead were abundantly enriched in NFMS fly ash and captured during HT-ESP. Whereas arsenic was widely dispersed throughout the whole analytical area. Specifically, the distribution of arsenic in the particles in hopper II and hopper III was more concentrated than that in hopper I (Fig. S3), which corresponded to the results reflected in Table 2.

The distribution characteristics of HMs in particles with different sizes at the outlet of HT-ESP were further analyzed. As shown in Fig. 6, copper and lead had similar distribution patterns on particles of different sizes, while the difference was the distribution of copper on particles <1 μm was very small. The distribution of arsenic on each particle size was more dispersed compared to copper and lead, while selenium was almost merely concentrated in $PM_{1.0}$ with a similar distribution pattern to arsenic. In general, lead was distributed in all particle sizes, copper was mainly distributed in $PM_{>10}$, while the volatile heavy metals arsenic and selenium had a large distribution in $PM_{1.0}$ and $PM_{1-2.5}$. The above conclusions were also supported by Table 2. The morphology of particles with various particle sizes didn't have significant discrepancies, large particles tended to be composed of small particles with flake and block structures (Fig. S4).

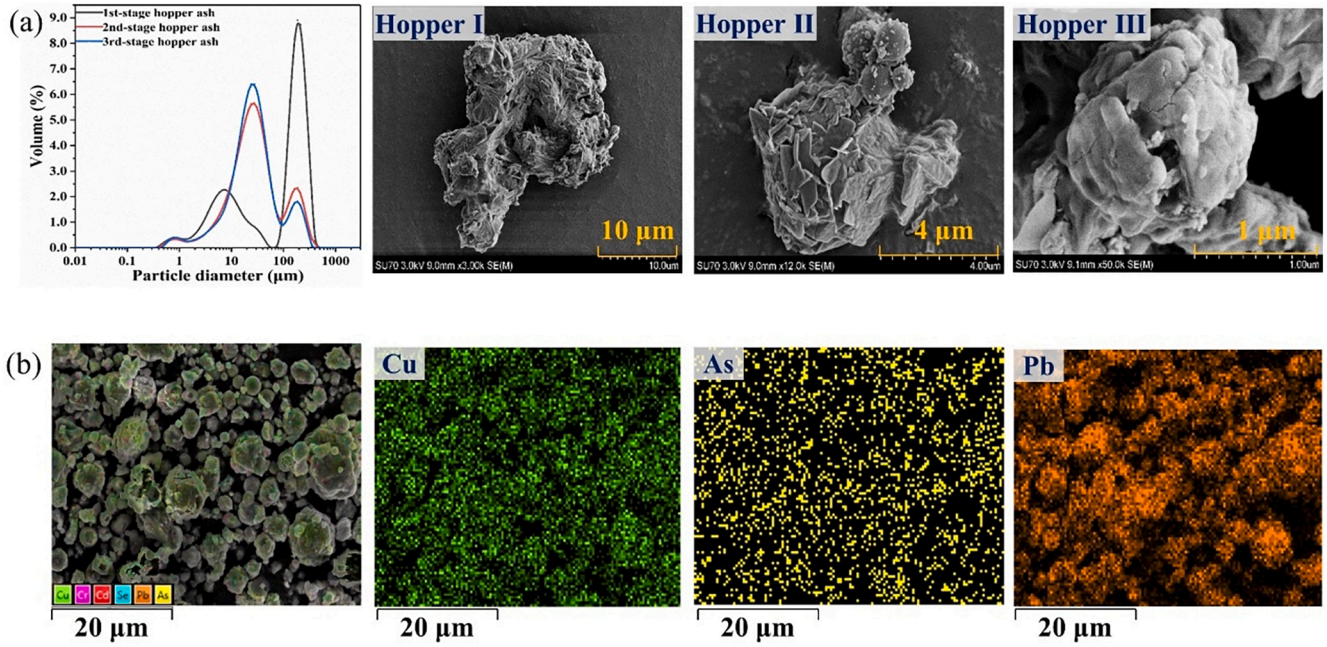

Fig. 5. Characteristics of the HT-ESP hopper ash: (a) size distribution and morphology of particles from different hoppers. (b) EDS mapping of high content HMs in hopper ash.

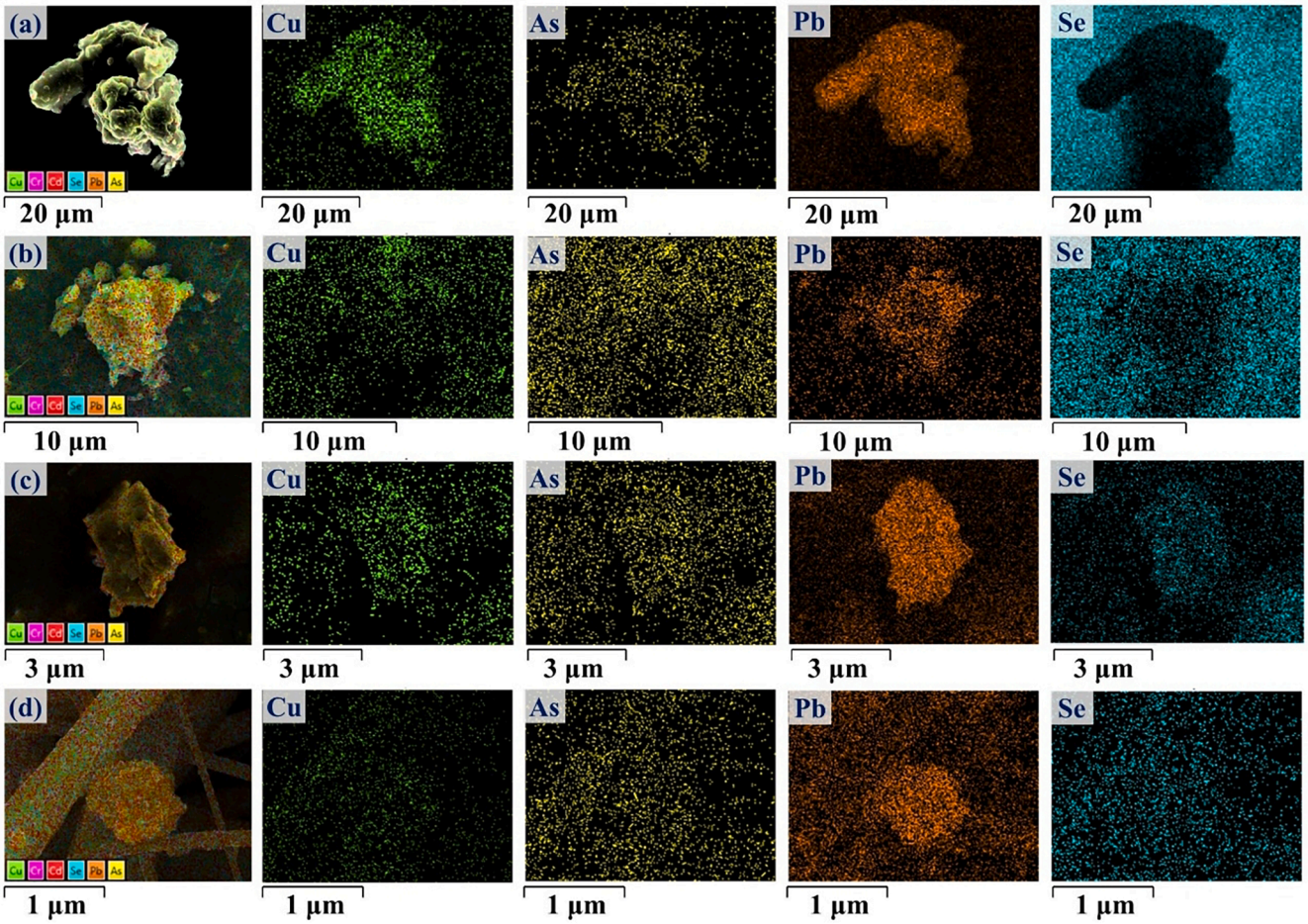

Fig. 6. HMs distribution in particles of different sizes at the outlet of HT-ESP. (a) $PM_{>10}$ (b) $PM_{2.5\text{-}10}$ (c) $PM_{1\text{-}2.5}$ (d) $PM_{1.0}$.

3.3. Collection and migration of HMs in the HT-ESP process.

To further investigate the migration of heavy metals in the solid and gas phase during the HT-ESP process, the same analytical method (ICP-MS) was conducted for the PM and flue gas absorbing solvent collected under rated operating conditions. The main heavy metal proportion of

Table 3
Typical mean TE proportion of PM at different locations in HT-ESP under rated conditions.

Inlet Temperature (K)	Outlet Temperature (K)	Location		Heavy metal proportion in fly ash (μg/g)			
				Cu	As	Pb	Se
572	437	Inlet		148523.4	69682.53	22595.03	31.43
		Outlet	$PM_{>10}$	171923.8	65892.26	25377.87	1426.57
			$PM_{2.5\text{-}10}$	173708.5	77338.17	28027.24	970.02
			$PM_{1\text{-}2.5}$	151865.2	83908.47	22897.88	2366.67
			$PM_{1.0}$	93490.55	79981.62	8640.11	4064.09
		Hopper		176717.6	88279.52	29330.04	490.63
573	445	Inlet		148523.4	69682.53	22595.03	31.43
		Outlet	$PM_{>10}$	174899.5	62698.94	24364.98	960.02
			$PM_{2.5\text{-}10}$	164734.2	73141.37	23255.16	1480.80
			$PM_{1\text{-}2.5}$	143587.8	79003.51	21653.89	2615.55
			$PM_{1.0}$	82000.59	75880.36	7890.21	3910.25
		Hopper		170525.9	85470.09	28902.37	430.52
575	454	Inlet		148523.4	69682.53	22595.03	31.43
		Outlet	$PM_{>10}$	169991.2	57533.50	23122.71	522.86
			$PM_{2.5\text{-}10}$	162394.5	63619.84	25862.86	797.28
			$PM_{1\text{-}2.5}$	159637.1	72198.15	20343.42	1246.82
			$PM_{1.0}$	71510.27	69560.68	7310.24	2740.90
		Hopper		165188.6	81323.01	27310.65	370.14
577	464	Inlet		148523.4	69682.53	22595.03	31.43
		Outlet	$PM_{>10}$	154762.6	53645.02	24412.86	402.37
			$PM_{2.5\text{-}10}$	153313.5	59629.87	21887.48	682.75
			$PM_{1\text{-}2.5}$	143445.1	68832.27	18740.90	914.30
			$PM_{1.0}$	62330.53	62480.98	6350.40	1300.87
		Hopper		163525.2	75478.92	26410.45	290.56

PM at different locations in HT-ESP under rated operating conditions was in this study (Table 3). The temperature difference between the inlet and outlet of the HT-ESP gradually decreased with the long-term operation. Due to the small variation of the inlet temperature of HT-ESP under rated operating conditions, it could be considered that the fluctuation of the smelting raw materials was small, therefore the average value of HMs in the collected inlet fly ash was adopted for analysis. Similarly, although there were differences in the TE distribution in the particles of the three hoppers, to acquire the concentration of HMs in the whole ash hopper under the same sampling flue gas flow, particles in the three hoppers were mixed in proportion and the mean value of the TE proportion in the ash hopper was obtained.

The results revealed that the proportion of copper, arsenic and lead in inlet particles was lower than that in outlet and hopper particles, whereas the proportion of selenium in outlet particles was significantly higher. And the enrichment of heavy metals in hopper and outlet particles gradually decreased as the temperature difference between the inlet and the outlet decreased, which proved the existence of HMs migration during the temperature range and also proved the significance of HT-ESP. In addition, the proportion of arsenic and selenium in the outflow particles fell in each particle size segment, and the proportion of arsenic in $PM_{1\text{-}2.5}$ was higher while selenium was more concentrated in $PM_{1.0}$. A reasonable explanation for this phenomenon was arsenic and selenium were volatile HMs, and they were easier to get into the gas phase. If there was a large temperature difference between the inlet and outlet sampling, arsenic and selenium were more likely to condense and adhere to small size particles with large specific surface areas. The variation trend of HMs in the ESP process was consistent with the reference [19].

Furthermore, based on the formula (4)~(9), the migration of typical HMs (Cu, As, Pb, Se) in the gas phase and particles during HT-ESP under rated operating conditions are shown in Table 4. The highest concentration of HMs in the gas phase was at the inlet of HT-ESP and the HMs concentration in hopper particles was significantly higher than that in the inlet. The reason could be explained that due to the temperature difference, part of the HMs originally enriched in the inlet gas phase condensed into particles, and these particles fell into the ash hopper after being captured, resulting in an increase in HMs enrichment in hopper particles. Especially for selenium, a large amount of selenium originally concentrated in the inlet gas phase migrated into the hopper particles, although the selenium proportion in hopper particles wasn't high (<600 μg/g). While the regularity of copper and lead migration was not evident probably owing to the higher temperature required for copper and lead to vaporize from solid to gas, leading to a small variation of copper and lead concentration in hopper particles and gas phase.

To describe the migration variation of HMs in particles and gas phase during HT-ESP more conveniently, the enrichment ratio of HMs in particles and gas phase (ER_s and ER_G) could be calculated as follows:

$$ER_S = \frac{C_{Si}}{C_{Si} + C_{Gi}} \times 100\% \tag{9}$$

$$ER_G = \frac{C_{Gi}}{C_{Si} + C_{Gi}} \times 100\% \tag{10}$$

Due to the continuous operation of the HT-ESP, the outlet temperature increased from 437 K to 464 K, and the temperature difference between the inlet and outlet decreased from 135 K to 112 K. The effect of temperature on the enrichment ratio (abbreviated as ER) of heavy metals is shown in Fig. 7. When the temperature difference narrowed to 23 K, the variation of copper and lead enrichment ratio in the hopper particles was similar and <1 %. While the ER_G of arsenic increased by 2.7 % (6.1 %—8.8 %) and the ER_G of selenium increased by 18.5 % (31.3 %—49.8 %), indicating that the volatile heavy metals originally enriched on hopper particles were more likely to migrate into the gas phase as temperature increased. Therefore, reducing the temperature difference under the premise of ensuring the collection efficiency was an effective method to reduce the enrichment of volatile heavy metals in hopper particles.

When the outlet temperature was 464 K (the difference between inlet and outlet was 112 K), the migration of HMs was considered to reach a steady state and the ER_S and ER_G at different locations of HT-ESP are illustrated in Fig. 8. The migration patterns of copper and lead were similar, 8.8 % of copper and 7.9 % of lead migrated from the gas phase to the hopper particles during the removal process of HT-ESP. In terms of the 5.5 % of copper and lead in the gas phase at the hopper position, about 65 % of them migrated into outlet particles due to the temperature drop, the proportion was slightly higher than the 60 % mentioned in

Table 4
Trace metal element migration during HT-ESP under rated operating conditions.

Inlet Temperature (K)	Outlet Temperature (K)	Location	Mass Concentration (g/m^3)	Concentration in fly ash (mg/m^3 (PM))				Concentration in gas phase (mg/m^3 (gas))			
				Cu	As	Pb	Se	Cu	As	Pb	Se
572	437	Inlet	27.36 ± 1.12	4063.6 ± 177.5	1932.9 ± 66.9	618.2 ± 21.3	0.86 ± 0.10	675.3 ± 32.8	326.5 ± 22.6	188.2 ± 27.5	15.44 ± 0.94
		Outlet	0.85 ± 0.15	144.2 ± 24.1	71.26 ± 12.62	23.46 ± 1.94	1.28 ± 0.12	77.57 ± 9.82	57.42 ± 6.57	13.17 ± 0.87	3.82 ± 0.15
		Hopper	26.51 ± 1.27	4517.1 ± 204.4	2130.7 ± 120.8	769.8 ± 18.39	11.2 ± 0.33				
573	445	Inlet	27.36 ± 1.12	4063.6 ± 177.5	1932.9 ± 66.9	618.2 ± 21.3	0.86 ± 0.10	675.3 ± 32.8	326.5 ± 22.6	188.2 ± 27.5	15.44 ± 0.94
		Outlet	0.96 ± 0.17	158.1 ± 27.2	74.25 ± 12.43	23.32 ± 1.56	1.03 ± 0.11	88.53 ± 9.63	62.23 ± 7.16	13.02 ± 0.63	4.77 ± 0.19
		Hopper	26.40 ± 1.29	4492.3 ± 219.3	2122.9 ± 116.8	770.1 ± 45.02	10.3 ± 0.21				
574	454	Inlet	27.36 ± 1.12	4063.6 ± 177.5	1932.9 ± 66.9	618.2 ± 21.3	0.86 ± 0.10	675.3 ± 32.8	326.5 ± 22.6	188.2 ± 27.5	15.44 ± 0.94
		Outlet	1.08 ± 0.21	164.9 ± 34.0	77.43 ± 14.53	23.68 ± 4.41	0.98 ± 0.08	96.51 ± 12.74	68.28 ± 6.83	13.75 ± 0.67	5.43 ± 0.32
		Hopper	26.28 ± 1.31	4477.5 ± 215.4	2113.7 ± 113.1	768.9 ± 35.78	9.72 ± 0.48				
576	464	Inlet	27.36 ± 1.12	4063.6 ± 177.5	1932.9 ± 66.9	618.2 ± 21.3	0.86 ± 0.10	675.3 ± 32.8	326.5 ± 22.6	188.2 ± 27.5	15.44 ± 0.94
		Outlet	1.22 ± 0.26	178.73 ± 40.22	82.17 ± 16.22	24.08 ± 4.87	0.92 ± 0.07	106.4 ± 15.3	77.86 ± 7.38	14.26 ± 1.26	7.60 ± 0.73
		Hopper	26.14 ± 1.37	4453.8 ± 224.1	2099.4 ± 117.2	768.1 ± 35.6	7.58 ± 0.39				

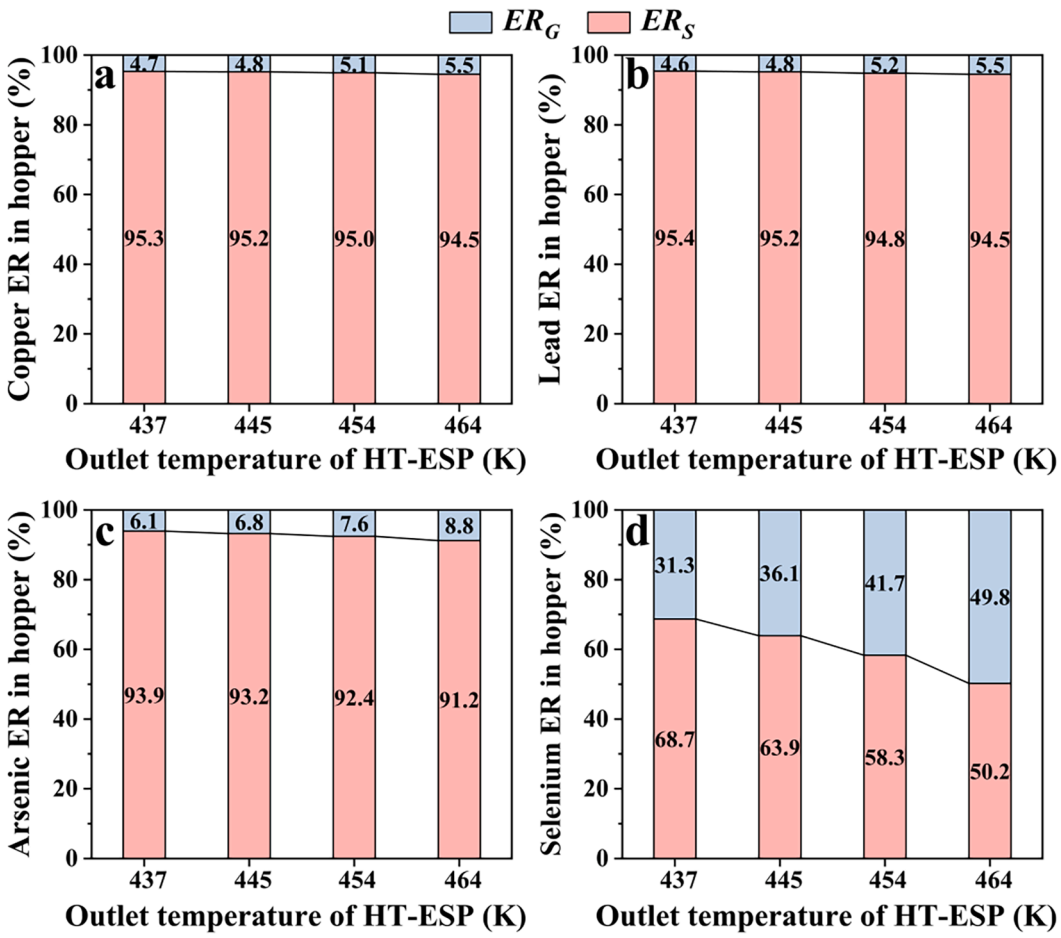

Fig. 7. Variation of ER_S and ER_G in ash hopper with the outlet temperature of HT-ESP. (a) Cu (b) Pb (c) As (d) Se.

reference [29]. The meaning of the red column represented the proportion of the solid phase and gas phase of heavy metals at the outlet migrated from the gas phase of heavy metals at the hopper. The ER_G of arsenic at the outlet was 44.7 %, indicating that the outlet temperature could allow a larger proportion of arsenic to keep in the gas phase, compared with copper and lead. Moreover, owing to the sampling temperature at the ash hopper was the lowest, which could be lower than the evaporation temperature of selenium, the ER_S of selenium at the hopper was nearly increased by 45 % compared with that at the inlet. The ER_G of selenium at the outlet was 89.0 %, and a high gas phase proportion could promote the HMs removal efficiency in the subsequent acid production process.

4. Conclusions

In this work, the removal characteristics of PM and the collection and migration of heavy metals in the HT-ESP process of copper smelting were investigated through an established pilot-scale platform. The following conclusions were drawn:

(1) There was an optimum flue gas velocity that could realize the highest particle collection efficiency of the HT-ESP. When the flow rate was 0.48 m/s and the maximum applied voltage was applied, the particle collection efficiency could reach 99.5 %. Among the captured outlet particles, the mass concentration of the $PM_{1.0}$ size segment was the highest.

(2) The distribution patterns of HMs at various particle sizes at the outlet were different. Lead was distributed in all particle sizes, copper was mainly distributed in $PM_{>10}$ and they were densely distributed on particles. Whereas the volatile heavy metals arsenic and selenium were mainly distributed in $PM_{1.0}$ and $PM_{1\text{-}2.5}$, and the distribution was relatively dispersed.

(3) As the temperature difference between the inlet and the outlet decreased, the proportion of heavy metals increased in each particle size segment of the outlet particles, and the volatile heavy metals were more likely to condense and adhere to small size particles with large specific surface area.

(4) With the long-term operation of the HT-ESP, the volatile heavy metals originally enriched on hopper particles were more likely to migrate into the gas phase, and the ER_G of arsenic and selenium increased by 2.7 % and 18.5 % respectively. Reducing the temperature difference under the premise of ensuring the collection efficiency was an effective method to reduce the enrichment of volatile heavy metals in hopper particles.

(5) The migration patterns of heavy metals were revealed: 8.8 % of copper, 7.9 % of lead, 8.3 % of arsenic and 45 % of selenium migrated from the gas phase into the hopper particles during the removal process of HT-ESP. These results could be helpful in the designing of novel processes for the separation of HMs in copper smelting flue gas and their further utilization.

CRediT authorship contribution statement

Zhicheng Wu: Writing – original draft, Conceptualization, Writing – review & editing. **Dingzhen Wang:** Methodology, Data curation. **YIfan Wang:** Validation, Supervision. **Lingyu Shao:** Formal analysis. **Yuzhong He:** Investigation, Project administration, Funding acquisition. **Hui Liu:** Validation. **Chenghang Zheng:** Project administration. **Xiang**

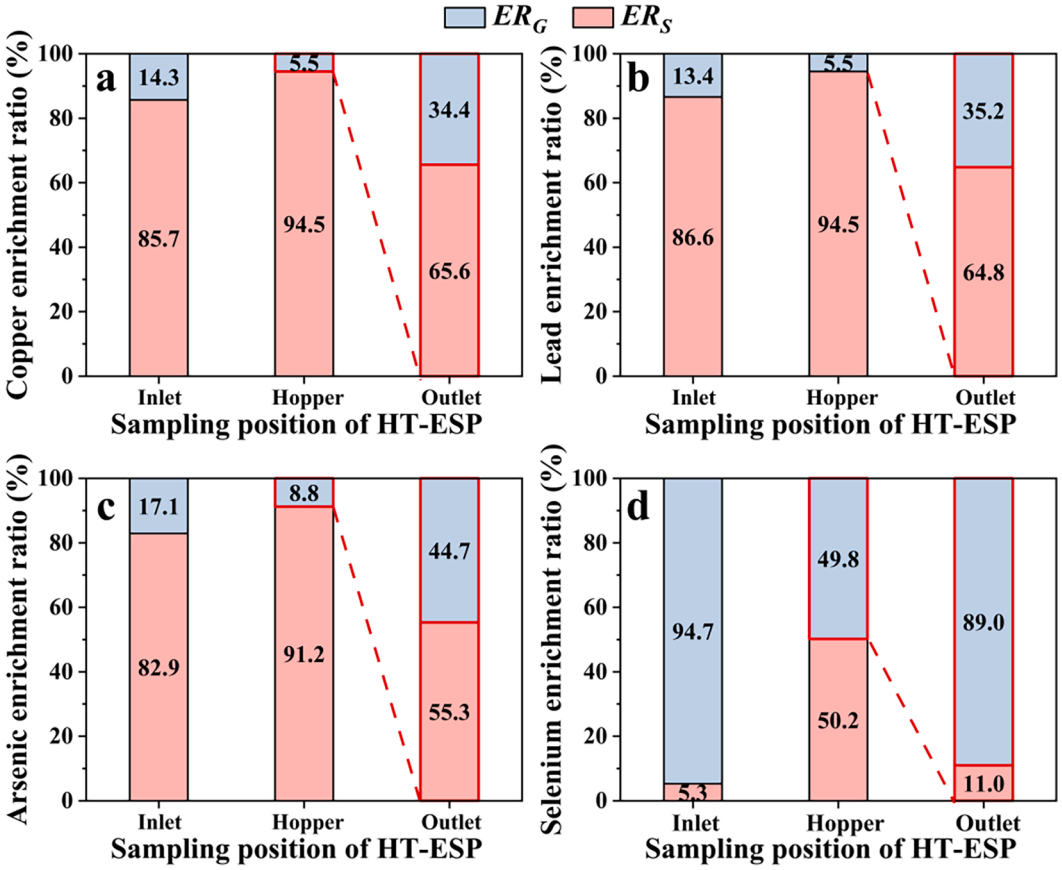

Fig. 8. HMs migration in particles and gas phase at different locations of HT-ESP. (a) Cu (b) Pb (c) As (d) Se.

Gao: Supervision, Funding acquisition.

Declaration of Competing Interest

The authors declare that they have no known competing financial interests or personal relationships that could have appeared to influence the work reported in this paper.

Data availability

The data that has been used is confidential.

Acknowledgments

This work was financially sponsored by the National Key Research and Development plan (2017YFC0210405), the National Natural Science Foundation (52076191), and Key Research & Development Plan of Shandong Province (2020CXGC011401).

Appendix A. Supplementary data

Supplementary data to this article can be found online at https://doi.org/10.1016/j.fuel.2022.125851.

References

[1] Tian HZ, Zhu CY, Gao JJ, Cheng K, Hao JM, Wang K, et al. Quantitative assessment of atmospheric emissions of toxic heavy metals from anthropogenic sources in China: historical trend, spatial distribution, uncertainties, and control policies. Atmos Chem Phys 2015;15:10127–47.
[2] Quan Z, Huang W, Liao Y, Liu W, Xu H, Yan N, et al. Study on the regenerable sulfur-resistant sorbent for mercury removal from nonferrous metal smelting flue gas. Fuel 2019;241:451–8.
[3] Kang M-J, Kwon YK, Yu S, Lee P-K, Park H-S, Song N. Assessment of Zn pollution sources and apportionment in agricultural soils impacted by a Zn smelter in South Korea. J Hazard Mater 2019;364:475–87.
[4] Feng Y-Y, Shi J-W, Zhong Y-Q, Han X-Y, Feng Y-C, Ren L. Pollution characteristics and health risk assessment of heavy metals in road dust from non-ferrous smelting parks. Huan jing ke xue= Huanjing kexue 2020;41:3547–55.
[5] Yao W, Min X, Li Q, Wang Q, Liu H, Liang Y, et al. Dissociation mechanism of particulate matter containing arsenic and lead in smelting flue gas by pyrite. J Cleaner Prod 2020;259:120875.
[6] Kan T, Strezov V, Evans TJ, Nelson PF. Trace element deportment and particle formation behaviour during thermal processing of iron ore: technical reference for risk assessment of iron ore processing. J Cleaner Prod 2015;102:384–93.
[7] Zhang W, Che J, Wen P, Xia L, Ma B, Chen J, et al. Co-treatment of copper smelting flue dust and arsenic sulfide residue by a pyrometallurgical approach for simultaneous removal and recovery of arsenic. J Hazard Mater 2021;416:126149.
[8] Jiang Z, Guo Z, Peng C, Liu X, Zhou Z, Xiao X. Heavy metals in soils around non-ferrous smelteries in China: Status, health risks and control measures. Environ Pollut 2021;282:117038.
[9] Kinnarinen T, Golmaei M, Jernström E, Häkkinen A. Removal of hazardous trace elements from recovery boiler fly ash with an ash dissolution method. J Cleaner Prod 2019;209:1264–73.
[10] Gao W, Wang Y, Zhang H, Guo B, Zheng C, Guo J, et al. A numerical investigation of the effect of dust layer on particle migration in an electrostatic precipitator. Aerosol Air Qual Res 2020;20:166–79.
[11] Zheng C, Liu X, Xu X, Yan P, Chang Q, Wang Y, et al. Experimental study on electrostatic removal of high-carbon particle in high temperature coal pyrolysis gas. Proc Combust Inst 2019;37:2959–65.
[12] Suhonen H, Laitinen A, Kortelainen M, Yli-Pirilä P, Koponen H, Tiitta P, et al. High temperature electrical charger to reduce particulate emissions from small biomass-fired boilers. Energies 2020;14(1):109.
[13] Xu X, Gao X, Yan P, Zhu W, Zheng C, Wang Y, et al. Particle migration and collection in a high-temperature electrostatic precipitator. Sep Purif Technol 2015;143:184–91.
[14] Zheng C, Wu Z, Shen Z, Zhang H, Wang Y, Gao W, et al. Particle capture in a high-temperature electrostatic precipitator with different electrode configurations. Powder Technol 2020;372:84–93.
[15] Suhonen H, Laitinen A, Kortelainen M, Koponen H, Kinnunen N, Suvanto M, et al. Novel fine particle reduction method for wood stoves based on high-temperature electric collection of naturally charged soot particles. J Cleaner Prod 2021;312:127831.

[16] Wang W, Cui L. Research status on dust removal technology for high temperature gas. IOP Conf Series: Earth Environ Sci 2021;826(1):012061.
[17] Yan P, Zheng C, Zhu W, Xu X, Gao X, Luo Z, et al. An experimental study on the effects of temperature and pressure on negative corona discharge in high-temperature ESPs. Appl Energy 2016;164:28–35.
[18] Yan P, Zheng C, Xiao G, Xu X, Gao X, Luo Z, et al. Characteristics of negative DC corona discharge in a wire–plate configuration at high temperatures. Sep Purif Technol 2015;139:5–13.
[19] Czech T, Marchewicz A, Sobczyk AT, Krupa A, Jaworek A, Sliwinski L, et al. Heavy metals partitioning in fly ashes between various stages of electrostatic precipitator after combustion of different types of coal. Process Saf Environ Prot 2020;133:18–31.
[20] Zhao S, Duan Y, Wang C, Liu M, Lu J, Tan H, et al. Migration behavior of trace elements at a coal-fired power plant with different boiler loads. Energy Fuels 2017;31:747–54.
[21] Zheng C, Wang L, Zhang Y, Zhang J, Zhao H, Zhou J, et al. Partitioning of hazardous trace elements among air pollution control devices in ultra-low-emission coal-fired power plants. Energy Fuels 2017;31:6334–44.
[22] Chen G, Sun Y, Yan B, Yang R, Liu B, Cheng Z, et al. Distribution of trace elements during coal Gasification: the effect of upgrading method. J Cleaner Prod 2018;190:193–9.
[23] Hower JC, Senior CL, Suuberg EM, Hurt RH, Wilcox JL, Olson ES. Mercury capture by native fly ash carbons in coal-fired power plants. Prog Energy Combust Sci 2010;36(4):510–29.
[24] Wang L, Zheng C, Zhang Y, Yue T, Weng W, Zhao H, et al. Speciation characteristics and mobility of trace elements across ultralow emission air pollution control devices. Energy Fuels 2017;31:13963–71.
[25] Wu Q, Sun X, Su Y, Wen M, Li G, Xu L, et al. Behavior of sulfur oxides in nonferrous metal smelters and implications on future control and emission estimation. Environ Sci Technol 2019;53:8796–804.
[26] Wang Q, Guo X, Tian Q, Chen M, Zhao B. Reaction mechanism and distribution behavior of arsenic in the bottom blown copper smelting process. Metals 2017;7(8):302.
[27] Mamyachenkov SV, Khanzhin NA, Anisimova OS, Karimov KA. Extraction of nonferrous metals and arsenic from thin dusts of copper fuel production by combined technology. Russ J Non-Ferrous Metals 2022;62:648–58.
[28] Aponte H, Mondaca P, Santander C, Meier S, Paolini J, Butler B, et al. Enzyme activities and microbial functional diversity in metal(loid) contaminated soils near to a copper smelter. Sci Total Environ 2021;779:146423.
[29] Zhang J, Sun X, Deng J, Li G, Li Z, Jiang J, et al. Emission characteristics of heavy metals from a typical copper smelting plant. J Hazard Mater 2022;424:127311.
[30] Chen Y, Zhao Z, Taskinen P, Liang Y, Ouyang H, Peng B, et al. Characterization of copper smelting flue dusts from a bottom-blowing bath smelting furnace and a flash smelting furnace. Metall Mater Trans B 2020;51:2596–608.
[31] Wu Z, Zhang H, Shao L, Wang Y, Gao W, Wang D, et al. Nonferrous metal flue gas purification based on high-temperature electrostatic precipitation. Process Saf Environ Prot 2021;154:202–10.
[32] Zheng C, Shen Z, Yan P, Zhu W, Chang Q, Gao X, et al. Particle removal enhancement in a high-temperature electrostatic precipitator for glass furnace. Powder Technol 2017;319:154–62.
[33] USEPA, Method 29: Determination of Metals Emissions from Stationary Sources, in, US Environmental Protection Agency, Washington, DC., 1999.
[34] Zhou H, Liu G, Zhang L, Zhou C, Mian MM, Cheema AI. Strategies for arsenic pollution control from copper pyrometallurgy based on the study of arsenic sources, emission pathways and speciation characterization in copper flash smelting systems. Environ Pollut 2021;270:116203.
[35] Montenegro V, Sano H, Fujisawa T. Recirculation of high arsenic content copper smelting dust to smelting and converting processes. Miner Eng 2013;49:184–9.
[36] Zhang W, Che J, Xia L, Wen P, Chen J, Ma B, et al. Efficient removal and recovery of arsenic from copper smelting flue dust by a roasting method: Process optimization, phase transformation and mechanism investigation. J Hazard Mater 2021;412:125232.